Science Advances
AAAS

advances.sciencemag.org/cgi/content/full/5/8/eaaw4515/DC1

Supplementary Materials for

Simultaneous implementation of resistive switching and rectifying effects in a metal-organic framework with switched hydrogen bond pathway

Zizhu Yao*, Liang Pan*, Lizhen Liu, Jindan Zhang, Quanjie Lin, Yingxiang Ye, Zhangjing Zhang*, Shengchang Xiang*, Banglin Chen*

*Corresponding author. Email: zzhang@fjnu.edu.cn (Z.Z.); scxiang@fjnu.edu.cn (S.X.); banglin.chen@utsa.edu (B.C.)

Published 2 August 2019, *Sci. Adv.* **5**, eaaw4515 (2019)
DOI: 10.1126/sciadv.aaw4515

This PDF file includes:

Fig. S1. Structure and electrical performance of FJU-23-H_2O single crystal.
Fig. S2. The microscopic image of the experimental setup.
Fig. S3. Variations of distance (H1w1⋯O31) and bond angle (O1w–H1w1⋯O11) under various dc voltages applied on the same one single crystal of FJU-23-H_2O along the *c* axis.
Fig. S4. Structure and electrical performance of FJU-23-D_2O single crystal.
Fig. S5. The characterization of FJU-23-H_2O.
Table S1. Selected bond lengths (Å) and bond angles (°) for O1w.
Table S2. Selected bond lengths (Å) and bond angles (°) for O3w.
Table S3. Performance parameters for some representative RRAMs.
Table S4. Crystal data and structure refinement for FJU-23-H_2O, FJU-23-D_2O, and FJU-23-H_2O under voltage sweeping on one single crystal.

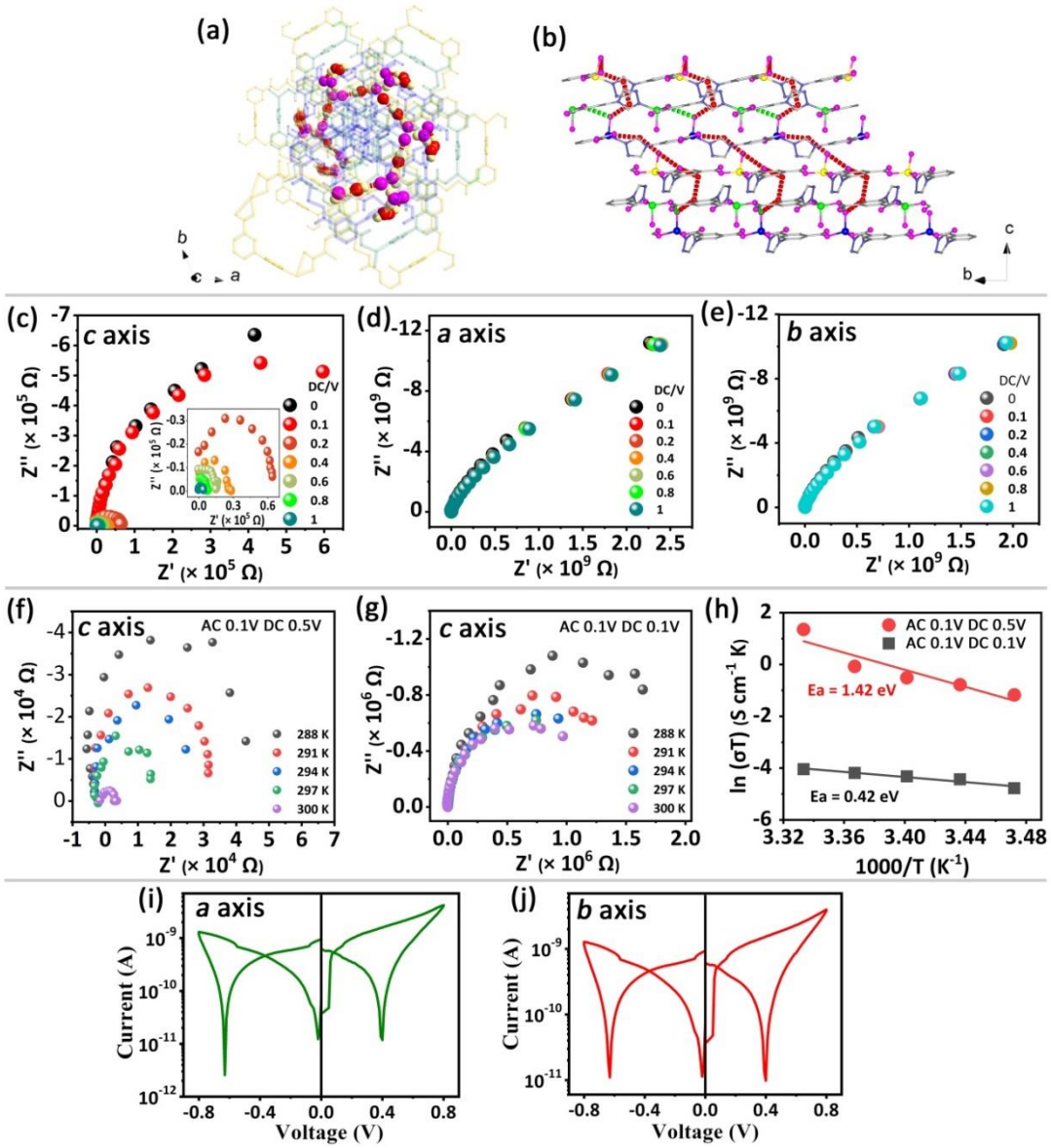

Fig. S1. Structure and electrical performance of FJU-23-H_2O single crystal. (**a**) The view of one discontinuous hydrogen-bonding chain in FJU-23-H_2O along the *c* axis. (**b**) The packing of six single honeycomb sheets. (**c**) Typical Nyquist plots of FJU-23-H_2O along the *c* axis under AC voltage of 0.1 V accompanying with various DC voltages. (**d** & **e**) Typical Nyquist plots under AC voltage of 1 V accompanying with various DC voltages for FJU-23-H_2O along the *a* and *b* axis. The temperature dependent of typical Nyquist plots for FJU-23-H_2O along the *c* axis under (**f**) AC voltage of 0.1 V, DC voltage of 0.5 V, and (**g**) AC voltage of 0.1 V, DC voltage of 0.1 V. (**h**) The Arrhenius plot of FJU-23-H_2O along the *c* axis. Semilogarithmic plot of the room-temperature current−voltage (I−V) characteristics of the single crystal FJU-23-H_2O along the *a* (**i**) and *b* (**j**) axes.

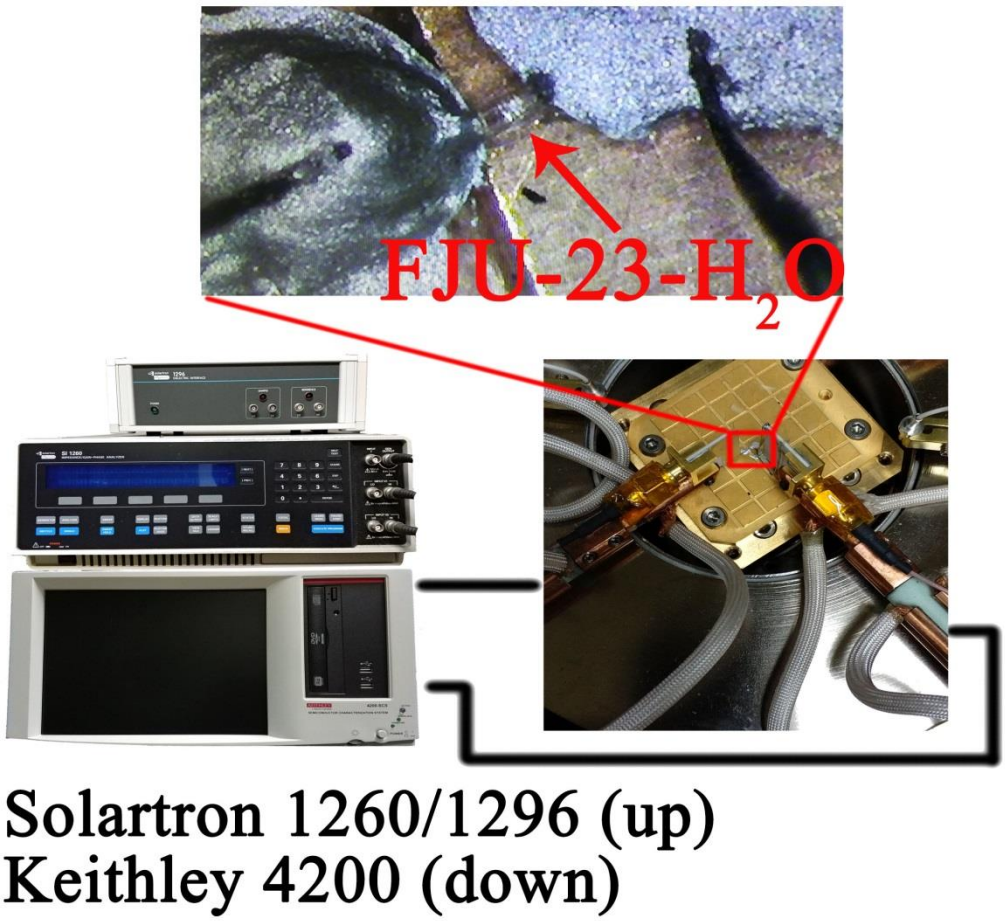

Fig. S2. The microscopic image of the experimental setup. Photo Credit: Zizhu Yao, Fujian Normal University.

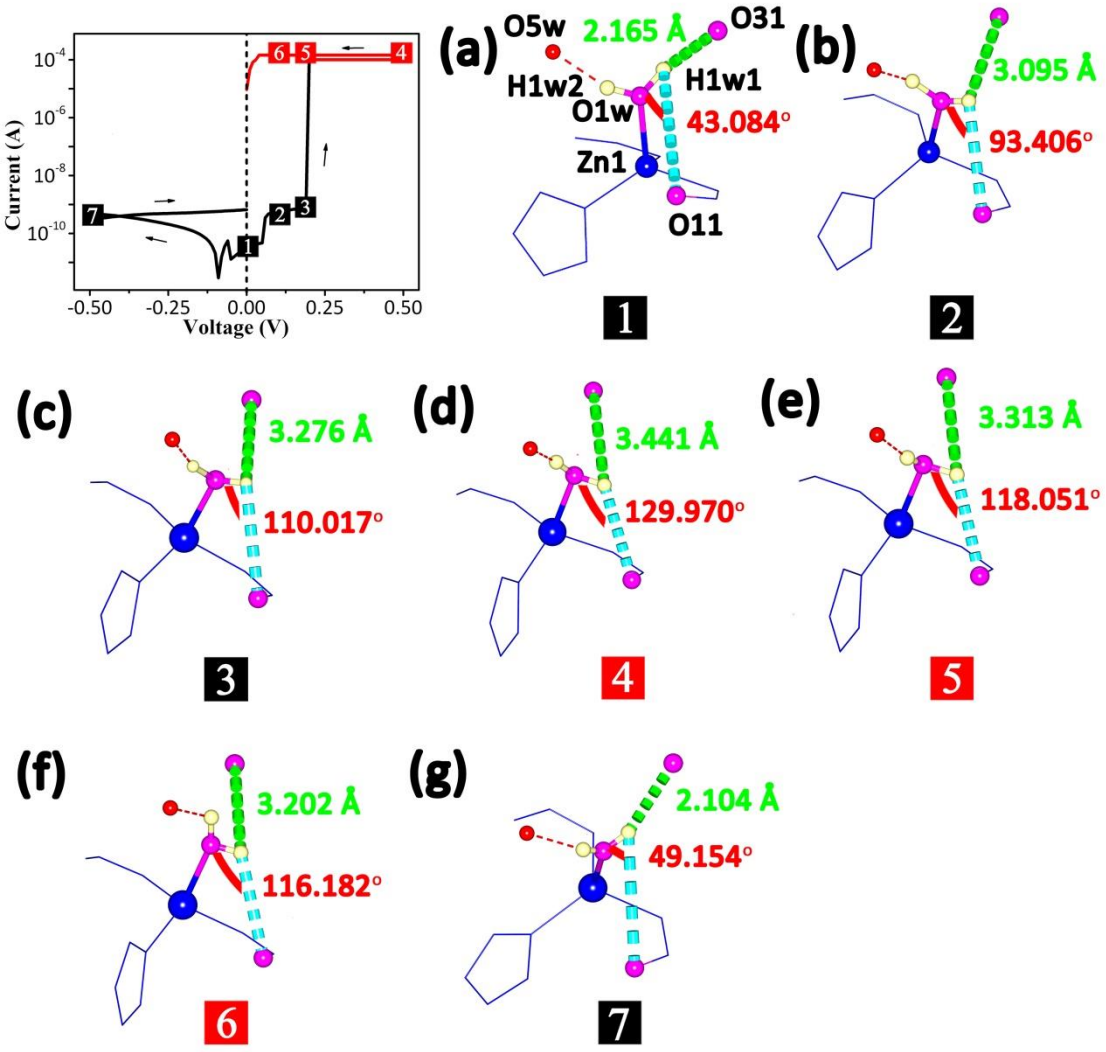

Fig. S3. Variations of distance (H1w1···O31) and bond angle (O1w–H1w1···O11) under various dc voltages applied on the same one single crystal of FJU-23-H_2O along the *c* axis.

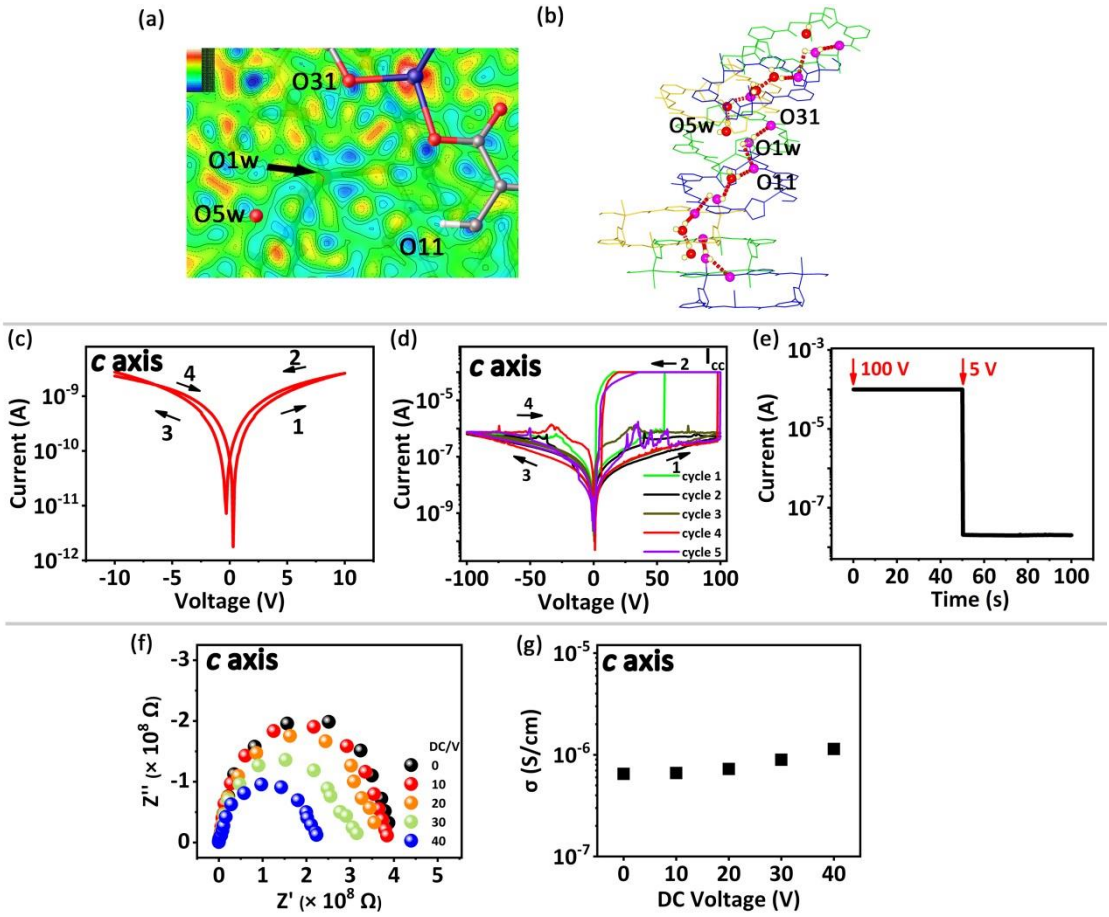

Fig. S4. Structure and electrical performance of FJU-23-D_2O single crystal. (**a**) The original difference Fourier maps (diff) near O1w before adding D1w1 and D1w2 in FJU-23-D_2O. (**b**) hydrogen-bonding chain fragment in FJU-23-D_2O. Semilogarithmic plots of the room-temperature current-voltage (I-V) characteristics of the FJU-23-D_2O along the *c* axis within the DC voltage range from -10 to 10 V (**c**) and -100 to 100 V (**d**). The arrows indicate the sweeping direction while the numbers represent the sweeping sequence; I_{CC} stands for the compliance current (10^{-4} A). The set voltage is 56.5, 97.0 and 99.5 V at cycle 1, 4 and 5, respectively. At cycles 2 and 3, resistive switching behavior has not been observed, which may be attributed to the higher set voltage than 100 V, exceeding the working limit of 100 V for our Keithley 4200 precision semiconductor parameter analyzer. (**e**) Volatile characteristics of FJU-23-D_2O. Its low resistance state under the bias of 100 V cannot be retained when the applied DC voltage is quickly switched down to 5 V. (**f**) Typical Nyquist plots and **(g)** proton conductivity calculated from AC impedance spectroscopy for FJU-23-D_2O along the *c* axis under AC voltage of 0.1 V accompanying with various DC voltages ranging from 0 to 40 V.

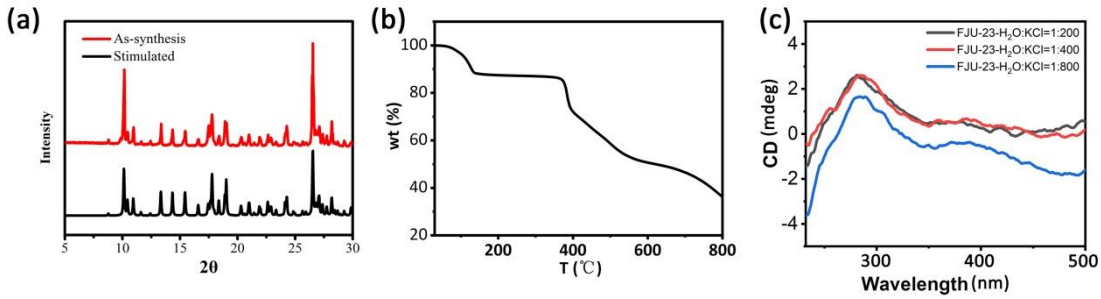

Fig. S5. The characterization of FJU-23-H_2O. (**a**) PXRD patterns, (**b**) TGA and (**c**) Circular dichroism spectra of FJU-23-H_2O.

Table S1. Selected bond lengths (Å) and bond angles (°) for O1w.

DC voltage/V	Angle(O1w-H1w1-O11)/°	Angle(H1w1-O1w-H1w2)/°	Angle(O1w-H1w1-O31)/°	d(O1w-O11)/Å	d(H1w1-O11)/Å	d(O1w-O31)/Å	d(H1w1-O31)/Å	d(O1w-O5w)/Å	d(O5w-H1w2)/Å
0	43.084(2)	118.710(6)	160.546(2)	3.189(8)	3.826(5)	3.102(8)	2.168(4)	2.570(8)	1.708(7)
0.1	93.406(3)	107.484(8)	82.931(4)	3.180(6)	3.019(6)	3.104(4)	3.095(7)	2.572(7)	1.511(8)
0.2	110.017(3)	100.000(8)	69.754(6)	3.181(7)	2.845(6)	3.097(6)	3.276(9)	2.571(6)	1.691(7)
0.5	129.970(5)	117.037(10)	59.891(6)	3.192(7)	2.549(6)	3.092(6)	3.441(7)	2.571(7)	1.654(9)
0.2	118.051(6)	115.076(10)	66.562(6)	3.189(8)	2.663(8)	3.067(7)	3.313(9)	2.585(9)	1.813(6)
0.1	116.182(3)	98.913(7)	74.216(4)	3.189(8)	2.751(4)	3.082(11)	3.202(5)	2.573(13)	1.910(18)
-0.5	49.154(9)	112.378(10)	162.628(15)	3.172(13)	3.691(15)	2.982(9)	2.104(9)	2.618(18)	1.803(13)

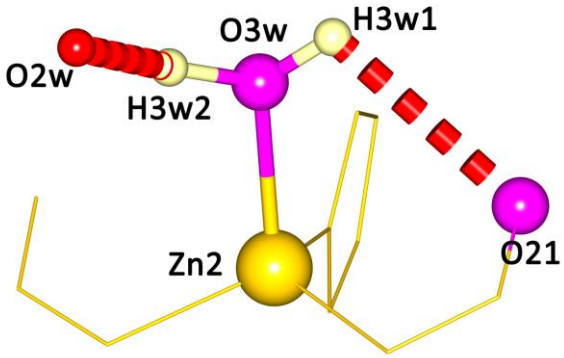

Table S2. Selected bond lengths (Å) and bond angles (°) for O3w.

	DC voltage /V	Angle (O3w-H3w1-O21)/°	d(O3w-H3w2) /Å	d(O3w-H3w1) /Å	d (O3w-O21) /Å
FJU-23-H_2O	0	103.847(5)	1.095(3)	0.928(5)	3.005(6)
FJU-23-0.1V	0.1	103.193(5)	0.912(5)	0.868(6)	3.001(5)
FJU-23-0.2V	0.2	106.267(5)	0.862(11)	0.898(4)	3.004(5)
FJU-23-0.5V	0.5	105.184(4)	0.861(5)	0.955(5)	3.013(6)
FJU-23-0.2V-R	0.2	106.392(3)	0.822(7)	1.041(3)	2.999(8)
FJU-23-0.1V-R	0.1	107.277(5)	1.010(9)	0.973(14)	2.998(10)
FJU-23-(-)0.5V	-0.5	106.814(3)	0.974(2)	0.926(13)	3.025(12)

Table S3. Performance parameters for some representative RRAMs.

RRAM	conductive carriers	on/off ratio	rectification ratio	set voltage (V)	Refs.
Ag/FJU-23-H_2O/Ag	H^+	2×10^5	10^5@±0.5 V	~0.2	this work
Au/mer-[Ru(2(phenylazo)pyridine)$_3$](PF_6)$_2$/ITO	Electron	~10^5	/	~0.4	10
Ag/ZIF-8 in MeOH vapor/Ag	Ag^+	~10^4	/	1.20-2.40	24
Ag/Rb-CD-MOF/Ag	OH^-	150	/	2	25
Ag/RSMOF-1/Ag	H^+	~30	/	7.5	26
rGO/MoS_2@ZIF-8/rGO	Electron, hole	7.0×10^4	/	3.3	29
Au/HKUST-1/Au	Cu^{2+}	18	/	~0.78	28
Cu/ ferrocene @HKUST-1/Au	/	~10	/	~0.6	27
Al/Zn-TCPP@PVPy/ITO	Electron	~10^3	/	0.5	30
Pt/Ta_2O_5/HfO_2/TiN	Electron	~10^3	10^4@±10 V	~5	33
Ag/a-Si/p-Si	Ag^+	10^3-10^7	10^4@±3 V	~4	34
Au/ZrO_2:Au-nanocystal/n^+-Si	oxygen vacancy	~10^2	7×10^2@±0.5 V	~3.1	35
Pt/NiO_x/TiO_x/Pt	Electron, hole	~10^6	~10^5@±3 V	~1.5	36
Pt /20 at.% SDC:STO VHN film (nominal thickness: 30nm) /Nb:STO	Electron, oxygen vacancy	~10^4	/	5	37
p-Si/SiO_2/n-Si	Si^{4+}	10^4	10^5@±4 V	~7	38
Au/PI:PCBM/Al/native SiO_x/p-Si	Electron	~10^2	10^4@±2.3 V	~3	39
Al/Glucose/p^+-Si	oxygen vacancy	~10^3	/	~3.4	40
Cu/poly(1,3,5-trivinyl-1,3,5-trimethyl cyclotrisiloxane) (pV3D3)/Al	Cu^{2+}	10^7	/	5	41

Table S4. Crystal data and structure refinement for FJU-23-H_2O, FJU-23-D_2O, and FJU-23-H_2O under voltage sweeping on one single crystal.

Compounds	FJU-23-H_2O	FJU-23-H_2O -293k	FJU-23-D_2O -293k	FJU-23-D_2O -150k	FJU-23-0.1V	FJU-23-0.2V	FJU-23-0.5V	FJU-23-0.2V-R	FJU-23-0.1V-R	FJU-23-(-)0.5V
Empirical formula	$C_{30}H_{29}N_9O_{19}Zn_3$	$C_{30}H_{29}N_9O_{19}Zn_3$	$C_{30}H_{15}D_{14}N_9O_{19}Zn_3$	$C_{30}H_{15}D_{14}N_9O_{19}Zn_3$	$C_{30}H_{29}N_9O_{19}Zn_3$	$C_{30}H_{29}N_9O_{19}Zn_3$	$C_{30}H_{29}N_9O_{19}Zn_3$	$C_{30}H_{29}N_9O_{19}Zn_3$	$C_{30}H_{29}N_9O_{19}Zn_3$	$C_{30}H_{29}N_9O_{19}Zn_3$
Formula weight	1015.73	1015.73	1029.82	1029.82	1015.73	1015.73	1015.73	1015.73	1015.73	1015.73
Temperature/K	150.0(10)	293.30(10)	293.00(7)	150.01(10)	150.0(10)	150.0(10)	150.0(10)	150.0(10)	150.0(10)	150.0(10)
Crystal system	hexagonal	hexagonal	hexagonal	hexagonal	hexagonal	hexagonal	hexagonal	hexagonal	hexagonal	hexagonal
Space group	$P6_5$	$P6_5$	$P6_5$	$P6_5$	$P6_5$	$P6_5$	$P6_5$	$P6_5$	$P6_5$	$P6_5$
a/Å	10.1796(2)	10.18518(13)	10.1919(4)	10.1943(2)	10.17833(15)	10.17716(19)	10.18058(19)	10.1798(2)	10.17920(17)	10.18156(17)
b/Å	10.1796(2)	10.18518(13)	10.1919(4)	10.1943(2)	10.17833(15)	10.17716(19)	10.18058(19)	10.1798(2)	10.17920(17)	10.18156(17)
c/Å	59.8076(12)	60.4220(9)	60.426(2)	59.8150(11)	59.8157(17)	59.8005(10)	59.8239(10)	59.8190(12)	59.8323(8)	59.5576(13)
α/°	90	90	90	90	90	90	90	90	90	90
β/°	90	90	90	90	90	90	90	90	90	90
γ/°	120	120	120	120	120	120	120	120	120	120
Volume/Å^3	5367.2(2)	5428.29(16)	5435.8(4)	5383.4(2)	5366.6(2)	5364.0(2)	5369.7(2)	5368.4(3)	5369.01(19)	5346.8(2)
Z	6	6	6	6	6	6	6	6	6	6
D_{calcd}(g/cm^3)	1.886	1.864	1.888	1.906	1.886	1.887	1.885	1.885	1.885	1.893
F(000)	3084.0	3084.0	3084.0	3084.0	3084.0	3084.0	3084.0	3084.0	3084.0	3084.0
Radiation	CuKα (λ = 1.54184 Å)	CuKα (λ = 1.54184 Å)	CuKα (λ = 1.54184 Å)	CuKα (λ = 1.54184 Å)	CuKα (λ = 1.54184 Å)	CuKα (λ = 1.54184 Å)	CuKα (λ = 1.54184 Å)	CuKα (λ = 1.54184 Å)	CuKα (λ = 1.54184 Å)	CuKα (λ = 1.54184 Å)
Reflections collected	10409	47429	20246	27486	16178	10283	10343	10408	20190	19769
Independent reflections	5187 [R_{int} = 0.0404, R_{sigma} = 0.0552]	7010 [R_{int} = 0.0825, R_{sigma} = 0.0427]	6243 [R_{int}= 0.0553, R_{sigma}= 0.0623]	6758 [R_{int}= 0.0616, R_{sigma}= 0.0494]	5609 [*R*int = 0.0365, *R*sigma = 0.0362]	4953 [*R*int = 0.0296, *R*sigma = 0.0358]	5130 [*R*int = 0.0284, *R*sigma = 0.0341]	4739 [*R*int = 0.0275, *R*sigma = 0.0337]	4641 [*R*int = 0.0316, *R*sigma = 0.0251]	5606 [*R*int = 0.0567, *R*sigma = 0.0396]
Goodness-of-fit on F^2	1.096	1.089	1.135	1.184	1.054	1.058	1.003	1.073	1.170	1.052
Final *R* indexes [I>=2σ (I)]	R_1= 0.0402, wR_2= 0.1072	R_1= 0.0580, wR_2= 0.1145	R_1= 0.0938, wR_2= 0.1921	R_1= 0.0808, wR_2= 0.1738	R_1= 0.0280, wR_2= 0.0624	R_1 = 0.0337, wR_2 = 0.0831	R_1 = 0.0288, wR_2 = 0.0666	R_1= 0.0372, wR_2= 0.0920	R_1 = 0.0377, wR_2 = 0.0950	R_1 = 0.0572, wR_2 = 0.1297
Final *R* indexes [all data]	R_1= 0.0452, wR_2= 0.1101	R_1= 0.0603, wR_2= 0.1151	R_1= 0.1006, wR_2= 0.1955	R_1= 0.0864, wR_2= 0.1756	R_1= 0.0297, wR_2= 0.0630	R_1 = 0.0343, wR_2 = 0.0837	R_1 = 0.0311, wR_2 = 0.0679	R_1= 0.0381, wR_2 = 0.0927	R_1 = 0.0389, wR_2 = 0.0953	R_1 = 0.0586, wR_2 = 0.1304
Largest diff. peak/hole / e Å^{-3}	0.55/-0.71	0.83/-0.0.83	1.16/-1.11	2.01/-0.98	0.46/-0.41	0.66/-0.59	0.37/-0.46	0.54/-0.56	0.84/-0.55	0.91/-0.64
Flack parameter	0.030(4)	0.02(2)	0.265(10)	0.039(16)	0.003(16)	0.00(3)	-0.030(19)	0.02(3)	-0.03(3)	-0.080(19)

$R1 = \sum(|F_o| - |F_c|) / \sum|F_o|$, $wR2 = [\sum w(F_o^2 - F_c^2)^2 / \sum w(F_o^2)^2]^{0.5}$